Evaluation of Batch and Equilibrium Cr^{6+} adsorption on Fe_3O_4 nanoparticles via isothermal and kinetic studies

Rimmy Singh (rimmisingh250@gmail.com)
DPG Institute of Technology and Management, Gurugram
Rachna Bhateria
Maharshi Dayanand University Rohtak

Research Article

Keywords: Hexavalent chromium, removal efficiency, isotherms, adsorption capacity, recovery

Posted Date: February 21st, 2022

DOI: https://doi.org/10.21203/rs.3.rs-1248502/v1

Abstract

Since many centuries, we have progressively tracked our capacities in the field of water contamination. An intense increase in heavy metals have led to the problems needing priority concerns. In this study, we have fabricated nanoparticles as an alternative source to decontaminate heavy metals from water. Hence, the efficacy of Fe_3O_4 nanoparticles was observed by adsorbing Cr^{6+} ions from aqueous systems. HRTEM analysis determined the average size of 42.90 nm and spherical morphology of the nanoparticles. Various parameters at their optimum conditions such as pH 2, contact time 50 minutes, temperature 20°C, initial metal concentration of 10 mgL^{-1} and nanoparticle dose of 60 mg were found to achieve maximum adsorption. Isotherms like Langmuir, Freundlich, Temkin and D-R were applied to the experimental equilibrium data, and it corresponds to the Temkin model with a correlation coefficient (R^2) of 0.99. Moreover, pseudo second order reaction describes the adsorption which was a three-step process. The negative value of ΔG well describes the physisorption nature, feasibility, and spontaneity of the adsorption process.

1. Introduction

Increasing global problem of pollution has threatened the world with future consequences. There is leapfrogging growth in contamination of potable water with heavy metals, organic compounds, dyes, and other such kind of pollutants. Amongst these global issues, heavy metal pollution has dominated the system. Heavy metals including, but not limited to lead, Chromium, Cadmium, Mercury, Arsenic etc. have contributed majorly and are responsible for severe health ailments. Accumulation of heavy metals in water and environment is the most urgent problem of water contamination needed to be prioritized before it's too late to act. Wastewater discharge from industrial and mining sources is responsible for the heavy metal pollution. Among various heavy metals, major focussed heavy metal is hexavalent chromium (Cr^{6+}) in wastewater [1, 2]. The use of chromate and dichromate in textile, paint, electroplating, metallurgy, leather tanning etc. industries have contributed high levels of Cr^{6+} in discharged effluents [1, 3]. The hexavalent form of chromium is 500 times more lethal and carcinogenic than trivalent form [4]. According to “United States Environmental Protection Agency (USEPA)”, the maximum permissible limit for Cr^{6+} discharge in surface water is 0.1 mgL^{-1} and in potable domestic water is 0.05 mgL^{-1} [5].

Highly toxic Chromium (Cr^{6+}) metal ion is regarded as the “carcinogenic, teratogenic and mutagenic” element to humans as well as animals [6]. Though there have been many technologies such as ion exchange, precipitation, chemical reduction etc. to remediate chromium and other heavy metals. But adsorption was found to be efficient method for removal of chromium from water and wastewater. Now, nanotechnology has entered the system with high profile properties and advantages over conventional adsorbents. Nanotechnology is the art of manipulating matter down to nanoscale (1-100 nm). Iron oxides nanoparticles (NPs) especially magnetite nanoparticles (Fe_3O_4 NPs) have been widely used for the adsorption of heavy metals [7, 8, 9, 10, 11, 12, 13]. Padmavathy et al. [14] synthesized Fe_3O_4 NPs for extracting Cr^{6+} ions from synthetic solution. Isotherm modelling on equilibrium data revealed that

Freundlich is the best fit for this work. In similar study, Fe_3O_4 nanoparticles were synthesized for the sorption of Cr^{6+} and Cr^{3+} ions from aqueous solution. The approximate size of Fe_3O_4 NPs was determined to be 22.4 ± 0.9 nm. Isothermal studies were carried out to find maximum capacity which were observed as 10.63 mg g^{-1} for Cr^{3+} ions and 3.46 mg g^{-1} for Cr^{6+} ions. Negative G and positive H values were determined by thermodynamic studies [15]. In comparison with activated carbon and clay, iron oxide nanoparticles have achieved favourable maximum adsorption capacity for removal and recovery of Cr^{6+} ions [16, 17]. It was observed that electrostatic attractions are considered weaker than chemical adsorption, hence, environmental conditions like pH, background ions and humic substances can affect adsorption. Therefore, consideration is needed while inspecting all these parameters during practical applications [18, 19, 20, 21].

In the present study, magnetite (Fe_3O_4) nanoparticles of spherical shape were fabricated by chemical reduction of ferric chloride. The synthesized nanoparticles were then characterized to know the structural and morphological characteristics of the NPs by employing Transmission Electron Microscopic techniques, X-Ray Diffraction and Energy Dispersive X-Ray spectroscopy. Batch experiments were conducted to determine the effect of pH, adsorbent dose, initial ion concentration, temperature and contact time on the removal of chromium from aqueous solution. Isotherm and kinetic studies were conducted to investigate the process and mechanism of chromium adsorption on magnetite nanoparticles. Thermodynamic parameters were also derived to observe the spontaneity and feasibility of adsorption.

2. Experimental

2.1 Chemical reagents and Instruments

Ferric chloride hexahydrate ($FeCl_3.6H_2O$) (98%), Sodium borohydride ($NaBH_4$), and Potassium dichromate ($K_2Cr_2O_7$) were used and were of analytical grade. Stock solutions (1000 mg L^{-1}, 100 mg L^{-1} and 50 mg L^{-1}) were processed from $K_2Cr_2O_7$ in double distilled water. By using pH meter (Mettler Toledo AG, FEP 20), the pH of the solution was measured and regulated accordingly by 0.1N HCl and 0.1N NaOH. “Inductively Coupled Plasma Mass Spectrometry (ICP-MS)” (Agilent’s 7900 ICP-MS) was used to detect the final concentrations of Cr^{6+} ions.

2.2 Synthesis of Fe_3O_4 nanoparticles

Chemical reduction method was used to prepare Fe_3O_4 NPs. Black precipitates of Fe_3O_4 were observed on addition of $NaBH_4$ in $FeCl_3.6H_2O$ solution. The synthesised NPs were washed with ethanol and calcined for 5 hours [22]. However, to confirm the composition and structure of nanoparticles, these were subjected to various characterization techniques.

2.3 Characterization techniques

The morphology of nanoparticles was characterized using High Resolution Transmission Microscopy (HRTEM- Tecnai G2 20) at 200KeV. The samples were ultrasonicated before exposing to the carbon coated copper grid. Elemental composition of magnetite nanoparticles was determined by Energy Dispersive Spectroscopy (EDS). Moreover, Selected Area Electron Diffraction (SAED) reveals the crystallinity of fabricated nanoparticles. X-Ray Diffraction (XRD) was used to study the crystal structure of the synthesized nanoparticles.

2.4 Batch Adsorption experiment

All batch experiments were performed to investigate the adsorption of Cr^{6+} on magnetite nanoparticles at 25°C with stirring speed of 200 rpm. For determining equilibrium pH, 20mg of adsorbent dose (magnetite nanoparticles) was added to 50 ml of 50 mg L^{-1} chromium stock solution at different pH ranging from 1-9 for 30 minutes. The pH was adjusted using HCl and NaOH. All experiments were conducted similarly by altering the parameter to be optimized and keeping all other parameters constant. ICP-MS (Agilent's 7900) was used to detect final concentration of Cr^{6+} ions in solution. The equilibrium adsorption capacity (q_e) of magnetite nanoparticles is "the amount of metal adsorbed per unit weight of adsorbent at equilibrium (mg g^{-1})" and was calculated from the equation given below:

$$q_e = \frac{(C_0 - C_e)V}{w}$$

1

initial Cr^{6+} ion concentration is denoted by C_0

equilibrium ion concentration by C_e

V is the volume of the solution (L),

W is the dry weight of Fe_3O_4 NPs.

The Cr6+ ion adsorption % was calculated by using given equation (2):

$$\text{Crremoval\%} = \frac{(\text{Co} - \text{Ce})}{Co} \times 100$$

2

Where, C_o and C_e are the Cr^{6+} ion concentrations (mg L^{-1}) at initial and equilibrium, respectively.

2.5 Equilibrium isotherms and kinetic analysis

About 70 years ago, Langmuir and Freundlich isotherms were firstly introduced and still they are the two mostly used adsorption isotherm equations. The success reason of their wider acceptability is their undoubted ability of fitting into an extensive range of data. In this study, Temkin and Dubinin-Radushkevich (D-R) isotherm was also applied to the obtained data. These isotherms were used as

mathematical tools to evaluate adsorption equilibrium of Cr^{6+} on magnetite nanoparticles. The adsorption equilibrium data was obtained at 25°C with pH 2 with agitation at 200 rpm. Pseudo first order, second order and intraparticle diffusion kinetic models were also used to fit the data [23, 24, 25].

3. Results And Discussion

3.1. Synthesis and characterization of iron oxide nanoparticles.

The morphology of magnetite nanoparticles was determined by High Resolution Transmission Electron Microscopy (HRTEM). The obtained images of synthesized nanoparticles at different magnification scales are shown in Figure 1(a-d). The fabricated nanoparticles were arranged in a beaded chain like structures with spherical morphology. The average size of the magnetite nanoparticles revealed by HRTEM was 42.90 nm. The polycrystalline nature of magnetite nanoparticles was confirmed by Selected Area Electron Diffraction Pattern (SAED) as shown in Figure 1(e). The Energy Dispersive X-Ray (EDX) peaks showed the constituents of the fabricated nanoparticles before and after Cr^{6+} adsorption (Figure 2a, b). The EDX composition includes the iron, oxygen, copper, and carbon peaks. The copper and carbon peaks were due to sample mounting on carbon coated copper grid. The X-Ray Diffraction (XRD) of the powdered magnetite nanoparticles give the structural information. The XRD pattern is shown in the Figure 3. The Fe_3O_4 nanoparticles possess orthorhombic structure with lattice constant (a) value of 2.799 A°. The XRD spectra showed multiple peaks at angle 2θ = 34.08, 38.47, 58.35, 83.99, 85.46 with hkl values of 023, 112, 006, 028, 173 (COD database, 96-900-2027) [26]. By using different peaks, crystallite size was determined by the following Scherer equation [27]:

$$D = \frac{k\lambda}{b\cos\theta}$$

3

Where D is the “crystallite size (nm)”, λ is the “wavelength (Cu Kα = 0.154)”, b is the “full width at half maxima” (rad) for diffraction peak, k is the constant having value equal to 0.9 and θ is the “diffraction angle in degrees”.

3.2 Batch experimental studies

3.2.1. Variation in pH

The solution pH gives an idea about the effect of functional groups of adsorbents, the solubility of metal ions, adsorbate’s degree of ionization and the counter ion concentration during the reaction [28]. Fe_3O_4 contains Fe^{2+} therefore, hydrolysis products such as $FeOH^+$, $Fe(OH)_2^0$, and $Fe(OH)_3^-$ varies with fluctuations in pH [29, 30, 31]. Different chromium species such as CrO_4^{2-}, $Cr_2O_7^{2-}$, $HCr_2O_7^-$, $HCrO_4^-$ commonly exists in aqueous solution. The Cr^{6+} removal decreases with increase in pH (as shown in

figure 4). The reason behind such behaviour may be the presence of more H^+ ions or $HCrO_4^-$ as major species at lower pH as OH^- groups are neutralised by H^+ ions and thus facilitates adsorption. At high pH, due to the presence of CrO_4^{2-}, $Cr_2O_7^{2-}$, abundance of OH^- species hinders the diffusion of dichromate ions and decreases the percent removal with increasing pH [32]. Hence, maximum adsorption was observed at pH 2 and minimum at pH 9.

3.2.2. Variation in initial ion concentration

Variation of initial ion concentration on Cr^{6+} removal was studied by adsorption on magnetite nanoparticles. The initial Cr^{6+} ion concentration was studied in the range of 10-60 mg L^{-1}. The results obtained were plotted in figure 5 and the maximum (88.3%) removal percentage was observed at 10 mg L^{-1}. The removal percent decreases with increase in concentration (also reported earlier by [33, 32]). However, according to the surface chemistry related theories, with increasing ionic strength an electric double layer decreases resulting in reduced adsorption of heavy metals [34].

3.2.3. Variation in adsorbent dose

The removal efficiency increases with increase in adsorbent dose with maximum at 60 mg and then decreases on increasing dose as shown in figure 6. However, no remarkable increase was observed in adsorption efficiency on further addition of dose upto 90 mg. The reason behind can be the aggregation of clustering nanoparticles on increasing NPs dose and hence, the availability of adsorption sites got reduced. As the same amount of Cr^{6+} ions got adsorbed on the larger surface area resulted in reduction of adsorption capacity [35].

3.2.4. Variation in contact time

To study the effect of contact time on adsorption, a range of 15-60 minutes was selected, and graph was plotted (Figure 7). On increasing agitation time, the Cr^{6+} removal also got increased. A maximum (75.3%) was observed at 50 minutes and removal percent decrease with increase in contact time. However, by increasing contact time, adsorption capacity got decreased.

3.2.5. Effect of temperature

Cr^{6+} adsorption was found to be decreased with increased temperature as represented by figure 8. The adsorption rate was increased suddenly from 15˚C to 20˚C and then declines with increasing temperature up to 40˚C. maximum Cr^{6+} removal was achieved at 20˚C and considered as optimum temperature. The decreased removal with increased temperature was possibly due to the tendency of Cr^{6+} ions to remain in the aqueous phase [36].

3.3. Isothermal Studies

Adsorption isotherms are “represented as the relation between number of adsorbate molecules per unit mass of adsorbent and the residual adsorbate concentration in bulk solution at a constant temperature”.

In this work, Langmuir, Freundlich, Temkin and D-R (Table 1) were evaluated by adsorption of Cr^{6+} on magnetite nanoparticles [37, 38, 39, 40, 41].

Langmuir isotherm describes the equilibrium between adsorbent and adsorbate where, adsorption process is limited to monolayer. It also describes the homogenous surface of adsorbent assuming that there are no sideways interactions between the nearby adsorbed molecules, where every molecule occupies a single adsorption site [42]. The Langmuir equation used is given below:

$$C_e/q_e = 1 / (K_L \times q_m) + C_e/q_m \quad (4)$$

Where, q_m is the Langmuir capacity and a plot between C_e/q_e vs C_e was used to calculate the value of constants as shown in Figure 9a. The Langmuir constant (K_L) and maximum adsorption capacity (q_m) can be derived from the above equation 4 (Table 1). The value of q_m derived from Langmuir modelling is 0.154 mg g^{-1}. Separation factor (R_L) is another parameter which evaluates the feasibility of Langmuir isotherm and can be derived from the following equation:

$$R_L = 1 / (1 + K_L \times C_o) \quad (5)$$

The R_L indicates the nature of isotherm, when R_L ▯ 1, then the adsorption is considered as unfavourable whereas when $R_L = 1$, there is a linear adsorption when $0 < R_L < 1$, there is favourable adsorption while $R_L = 0$, adsorption is irreversible

The R_L value for magnetite nanoparticles was found to be 0.767, which is less than one and showed potential interaction among Fe_3O_4 nanoparticles and Cr^{6+} ions.

The adsorption data was further evaluated to fit Freundlich isotherm equation. This model facilitates the heterogenous surface adsorption forming multilayers on the surface [43]. The Freundlich model equation is given below:

$$\ln q_e = \ln K_f + 1/n \ln C_e \quad (6)$$

where, "K_f and n are the Freundlich constants". The graph plot between $\ln q_e$ vs $\ln C_e$ (Figure 9b) gives the value of K_f (0.459) and n (18.28) (Table 1). The lower the value of 1/n (0.054) and higher value of n denotes efficient interactions among magnetite nanoparticles and chromium.

Temkin model was also evaluated for description of equilibrium mechanism by considering adsorbent-adsorbate interactions. The Temkin equation given below:

$$qe = (R_T/B_T) \times \ln (A_T \times C_e) \quad (7)$$

gives the value of equilibrium binding constant (A_T) and Temkin constant (B_T). A curve was plotted q_e vs $\ln C_e$ (Figure 9c) to get the linear equation and find the values of constant. The value of B_T is 24.33 kJ

mol^{-1} which is the heat of adsorption, further the value of B_T greater than 20 kJ mol^{-1} is the feature of physisorption.

D-R model is based upon multilayer adsorption model involving Van der Waal forces. It expresses adsorption mechanism with gaussian energy distribution onto heterogenous surfaces [44]. The equation to derive D-R parameters is given below:

$\ln q_e = \ln q_m - K\epsilon^2$ (8)

$\epsilon = RT \times \ln [1+ (1/Ce)]$ (9)

$$E_m = \frac{1}{\sqrt{2K}}$$

10

The curve was plotted against $\ln q_e$ vs ϵ^2 (Figure 10d). From D-R model, the value of q_m was 4.89 mg g^{-1}, this shows the maximum monolayer value of chromium adsorption per unit weight of adsorbent. The "value of mean free energy (E_m)" is 1.46 kJ mol^{-1} at 293 K. In D-R isotherm, adsorption can be one of these three conditions i.e. if E_m < 8.0 kJ mol^{-1}, it is physisorption, E_m = 8.0-16.0 kJ mol^{-1} then it is ion exchange while if E_m 16-400 kJ mol^{-1}, it is chemisorption. Hence, it is assumed that "process and concentrations of adsorbate and adsorbent are involved in rate determining step and the adsorption is physisorption" according to this model.

Based on correlation value of the experimental data the best fit model were compared and R^2 order of the adsorption is Temkin Langmuir D-R Freundlich.

3.4. Adsorption kinetics

The adsorption data was analysed for kinetics study of chromium removal by Pseudo first order, second order kinetics and intraparticle diffusion (Table 2). The adsorption kinetic model estimates the rate and mechanism of adsorption reactions.

First order kinetic equation describes "the solute adsorption on the adsorbent surface". The linear form of first order kinetics is given as follows:

$\ln(q_e-q_t) = \ln q_e - k_1 t$ (11)

A curve was plotted, $\log(q_e-q_t)$ against t to find the values of k_1 and q_e (Figure 10a). A linearized form of pseudo second order equation is:

$t/q_t = 1/(k_2 qe^2) + (1/q_e)\, t$ (12)

The value of rate constant k_2 (0.985) was derived by plotting a curve between t/qt vs t (Figure 10b) and are summarized in Table 3. The correlation coefficient (R^2) of Lagergren's first order and second order was found to be 0.68 and 0.98 respectively. Hence, pseudo second order kinetic model was the best fit to the experimental data.

Intraparticle diffusion model describes the adsorbate intraparticle uptake and pore diffusion during adsorption process. The linear equation for intraparticle model is:

$q_t = k_i \sqrt{t} + x_i$ (13)

A curve for intraparticle diffusion model (Figure 10c) gives the value of X_i (0.076) at 293 K for 10 mg L^{-1} Cr^{6+} solution. The boundary layer effect is directly proportional to the value of X_i i.e. higher the X_i value, higher will be the boundary layer effect.

The adsorption of Cr^{6+} on magnetite nanoparticles is a three-step process which involves the transportation of Cr^{6+} ions to the surface of Fe_3O_4 nanoparticles from bulk solution. Secondly, Cr^{6+} diffusion to the interior of the Fe_3O_4 pores. And ultimately adsorption of Cr^{6+} onto active sites of Fe_3O_4 nanoparticles surface [45].

3.4.4. Thermodynamics of adsorption

To assess the adsorption feasibility and spontaneity, thermodynamic parameters have wide role to play as they give basic information to design adsorption process. Feasibility and spontaneity are governed by parameters such as entropy (ΔS°), heat of enthalpy (ΔH°) and Gibbs free energy (ΔG°). various equations were used to calculate the thermodynamic parameters of this adsorption process which were given as follows [46, 47, 48]:

Distribution coefficient can be calculated by the equation,

$\ln K_d = \Delta S/R - \Delta H/RT$ (14)

where $K_d = q_e/C_e$ (15)

Equilibrium chromium concentration is given by, $\ln C_e = -\ln K_0 + \Delta H/RT$ (16)

$\Delta G = \Delta H - T\Delta S$ (17)

By plotting a curve between $\ln K_d$ vs 1/T and $\ln C_e$ vs 1/T (Figure 11a and 11b respectively) values of thermodynamic parameters were calculated (Table 3) from slope and intercept of obtained equation.

The adsorption of chromium on magnetite nanoparticles was observed to favour lower temperature. With increase in temperature, the adsorption rate decreases due to weak adsorbate-adsorbent interactions. The negative value of ΔG° is evident to feasibility and spontaneity of the adsorption process at a given

temperature. The physisorption mechanism of adsorption was confirmed by the negative value of ΔH° which lie in the range of -20 to 40 kJ mol^{-1} [49]. However, the positive ΔS° value suggests spontaneous adsorption.

3.5 Desorption studies

Recovery of adsorbent for reuse keep the process cost low. The adsorbent effeciecy of adsorption and desorption was studied by conducting three adsorption and desorption cycles. In case of Cr^{6+}, all the three cycles were observed to achieve 82%, 78% and 75% adsorption whereas desorption rate achieved was 80.2%, 75.8% and 68% as shown in Figure 12. For desorption of chromium 0.005 M of NaOH was used to separate chromium from nanoparticles.

Conclusion

The present experimental study investigates the chromium adsorption efficiency onto Fe_3O_4 NPs. The sodium borohydride chemical reduction route was used to produce Fe_3O_4 NPs. The nanoparticles have maximum adsorption capacity of 0.15mg/g at pH 2. The adsorption equilibrium, thermodynamics and kinetics of chromium adsorption was analysed. The Langmuir, Freundlich, Temkin and D-R isotherm equations were applied to find the best model. According to kinetic studies, Pseudo second order model was in good agreement with the obtained data and best fit. The change in Gibbs free energy was found to be negative which indicates the feasibility and spontaneity of the adsorption.

Declarations

Conflict of Interest

The authors declare that they have no conflict of interest.

References

1. Aydın YA, Aksoy ND (2009) Adsorption of chromium on chitosan: Optimization, kinetics and thermodynamics. Chem Eng J 151(1–3):188–194
2. Hena S (2010) Removal of chromium hexavalent ion from aqueous solutions using biopolymer chitosan coated with poly 3-methyl thiophene polymer. J Hazard Mater 181(1–3):474–479
3. Tanhaei B, Ayati A, Sillanpää M (2019) Magnetic xanthate modified chitosan as an emerging adsorbent for cationic azo dyes removal: Kinetic, thermodynamic and isothermal studies. Int J Biol Macromol 121:1126–1134
4. Dubey SP, Gopal K (2007) Adsorption of chromium (VI) on low cost adsorbents derived from agricultural waste material: a comparative study. J Hazard Mater 145(3):465–470
5. Sivakami MS, Gomathi T, Venkatesan J, Jeong HS, Kim SK, Sudha PNPreparation and characterization of nano chitosan for treatment wastewaters *Int. J.Biol. Macromol. 57*,204–12

6. Beheshti H, Irani M, Hosseini L, Rahimi A, Aliabadi M (2016) Removal of Cr (VI) from aqueous solutions using chitosan/MWCNT/Fe3O4 composite nanofibers-batch and column studies. Chem Eng J 284:557–564
7. Minh Tri P, Khim KS, Hidajat K, Uddin MS (2009) Surface functionalized nano-magnetic particles for wastewater treatment: adsorption and desorption of mercury. J Nanosci Nanotechnol 9(2):905–908
8. Huang YF, Li Y, Jiang Y, Yan XP (2010) Magnetic immobilization of amine-functionalized magnetite microspheres in a knotted reactor for on-line solid-phase extraction coupled with ICP-MS for speciation analysis of trace chromium. J Anal At Spectrom 25(9):1467–1474
9. Mandel K, Hutter F, Gellermann C, Sextl G (2012) Modified superparamagnetic nanocomposite microparticles for highly selective HgII or CuII separation and recovery from aqueous solutions. ACS Appl Mater Interfaces 4(10):5633–5642
10. Liu Y, Wang Y, Zhou S, Lou S, Yuan L, Gao T, Wu X, Shi X, Wang K (2012) Synthesis of high saturation magnetization superparamagnetic Fe3O4 hollow microspheres for swift chromium removal. ACS Appl Mater Interfaces 4(9):4913–4920
11. Hakami O, Zhang Y, Banks CJ (2012) Thiol-functionalised mesoporous silica-coated magnetite nanoparticles for high efficiency removal and recovery of Hg from water. Water Res 46(12):3913–3922
12. Gupta VK, Nayak A (2012) Cadmium removal and recovery from aqueous solutions by novel adsorbents prepared from orange peel and Fe2O3 nanoparticles. Chem Eng J 180:81–90
13. Dui J, Zhu G, Zhou S (2013) Facile and economical synthesis of large hollow ferrites and their applications in adsorption for As (V) and Cr (VI). ACS Appl Mater Interfaces 5(20):10081–10089
14. Padmavathy KS, Madhu G, Haseena PV (2016) A study on effects of pH, adsorbent dosage, time, initial concentration and adsorption isotherm study for the removal of hexavalent chromium (Cr (VI)) from wastewater by magnetite nanoparticles. Procedia Technol 24:585–594
15. Luther S, Brogfeld N, Kim J, Parsons JG (2013) Study of the thermodynamics of chromium (III) and chromium (VI) binding to iron (II/III) oxide or magnetite or ferrite and magnanese (II) iron (III) oxide or jacobsite or manganese ferrite nanoparticles. J Colloid Interface Sci 400:97–103
16. Hu J, Chen G, Lo IM (2005) Removal and recovery of Cr (VI) from wastewater by maghemite nanoparticles. Water Res 39(18):4528–4536
17. Hu J, Lo IM, Chen G (2007a) Performance and mechanism of chromate (VI) adsorption by δ-FeOOH-coated maghemite (γ-Fe2O3) nanoparticles. Sep Purif Technol 58(1):76–82
18. Hu J, Lo IM, Chen G Removal of Cr (VI) by magnetite Water Sci (2004) Technol 50(12):139–146
19. Hu J, Lo IM, Chen G (2007b) Comparative study of various magnetic nanoparticles for Cr (VI) removal. Sep Purif Technol 56(3):249–256
20. Yang W, Kan AT, Chen W, Tomson MB (2010) pH-dependent effect of zinc on arsenic adsorption to magnetite nanoparticles. Water Res 44(19):5693–5701

21. Yantasee W, Warner CL, Sangvanich T, Addleman RS, Carter TG, Wiacek RJ, Fryxell GE, Timchalk C, Warner MG (2007) Removal of heavy metals from aqueous systems with thiol functionalized superparamagnetic nanoparticles. Environ Sci Technol 41(14):5114–5119
22. Yuvakkumar R, Elango V, Rajendran V, Kannan N (2011) Preparation and characterization of zero valent iron nanoparticles. Digest journal of nanomaterials and biostructures 6(4):1771–1776
23. Sivaraj R, Namasivayam C, Kadirvelu K (2001) Orange peel as an adsorbent in the removal of acid violet 17 (acid dye) from aqueous solutions. Waste Manage 21(1):105–110
24. Sağ Y, Aktay Y (2002) Kinetic studies on sorption of Cr (VI) and Cu (II) ions by chitin, chitosan and Rhizopus arrhizus. Biochem Eng J 12(2):143–153
25. Dima JB, Zaritzky N (2017) Performance of Chitosan Micro/Nanoparticles to Remove Hexavalent Chromium from Residual Water. In Advanced Nanomaterials for Water Engineering,Treatment, and Hydraulics262–288
26. Fei Y, Frost DJ, Mao HK, Prewitt CT, Haeusermann D (1999) In situ structure determination of the high-pressure phase of Fe3O4. American Mineralogist 84(1–2):203–206
27. Yuan P, Fan M, Yang D, He H, Liu D, Yuan A, Zhu J, Chen T (2009) Montmorillonite-supported magnetite nanoparticles for the removal of hexavalent chromium [Cr (VI)] from aqueous solutions. J Hazard Mater 166(2–3):821–829
28. Kumari M, Pittman CU Jr, Mohan D (2015) Heavy metals [chromium (VI) and lead (II)] removal from water using mesoporous magnetite (Fe3O4) nanospheres. J Colloid Interface Sci 442:120–132
29. Cornell RM, Schwertmann U (2003) The iron oxides: structure, properties, reactions, occurrences and uses. John Wiley & Sons
30. Chowdhury SR, Yanful EK, Pratt AR (2012) Chemical states in XPS and Raman analysis during removal of Cr (VI) from contaminated water by mixed maghemite–magnetite nanoparticles. J Hazard Mater 235:246–256
31. Rajput S, Pittman CU Jr, Mohan D (2016) Magnetic magnetite (Fe3O4) nanoparticle synthesis and applications for lead (Pb2+) and chromium (Cr6+) removal from water. J Colloid Interface Sci 468:334–346
32. Sharma YC, Srivastava V (2011) Comparative studies of removal of Cr (VI) and Ni (II) from aqueous solutions by magnetic nanoparticles. J Chem Eng Data 56(4):819–825
33. Sharma YC, Srivastava V, Weng CH, Upadhyay SN (2009) Removal of Cr (VI) from wastewater by adsorption on iron nanoparticles. Can J Chem Eng 87(6):921–929
34. Onyancha D, Mavura W, Ngila JC, Ongoma P, Chacha J (2008) Studies of chromium removal from tannery wastewaters by algae biosorbents, Spirogyra condensata and Rhizoclonium hieroglyphicum. J Hazard Mater 158(2–3):605–614
35. Ren G, Wang X, Huang P, Zhong B, Zhang Z, Yang L, Yang X (2017) Chromium (VI) adsorption from wastewater using porous magnetite nanoparticles prepared from titanium residue by a novel solid-phase reduction method. Sci Total Environ 607:900–910

36. Sari A, Tuzen M (2008) Biosorption of total chromium from aqueous solution by red algae (Ceramium virgatum): equilibrium, kinetic and thermodynamic studies. J Hazard Mater 160(2–3):349–355
37. Foo KY, Hameed BH (2010) Insights into the modeling of adsorption isotherm systems. Chem Eng J 156(1):2–10
38. Wang A, Zhou K, Liu X, Liu F, Chen Q (2017) Development of Mg–Al–La tri-metal mixed oxide entrapped in alginate for removal of fluoride from wastewater. RSC adv 7(50):31221–31229
39. Ma A, Ke F, Jiang J, Yuan Q, Luo Z, Liu J, Kumar A (2017) Two lanthanide-based metal–organic frameworks for highly efficient adsorption and removal of fluoride ions from water. Cryst Eng Comm 19(16):2172–2177
40. Tassist A, Lounici H, Abdi N, Mameri N (2010) Equilibrium, kinetic and thermodynamic studies on aluminum biosorption by a mycelial biomass (Streptomyces rimosus). J Hazard Mater 183(1–3):35–43
41. Hussain Z, Daosheng L, Xi L, Jianxiong K (2015) Defluoridation by a Mg–Al–La triple-metal hydrous oxide: synthesis, sorption, characterization and emphasis on the neutral pH of treated water. RSC Adv 5(55):43906–43916
42. Liu L, Luo XB, Ding L, Luo SL (2019) Application of nanotechnology in the removal of heavy metal from water. In Nanomaterials for the Removal of Pollutants and Resource Reutilization. 83-147
43. Vasiliu S, Bunia I, Racovita S, Neagu V (2011) Adsorption of cefotaxime sodium salt on polymer coated ion exchange resin microparticles: kinetics, equilibrium and thermodynamic studies. Carbohydr Polym 85(2):376–387
44. Celebi O, Üzüm Ç, Shahwan T, Erten HN (2007) A radiotracer study of the adsorption behavior of aqueous Ba2+ ions on nanoparticles of zero-valent iron. J Hazard Mater 148(3):761–767
45. Tehrani-Bagha AR, Nikkar H, Mahmoodi NM, Markazi M, Menger FM (2011) The sorption of cationic dyes onto kaolin: Kinetic, isotherm and thermodynamic studies. Desalination 266(1–3):274–280
46. Li H, Huang G, An C, Hu J, Yang S (2013) Removal of tannin from aqueous solution by adsorption onto treated coal fly ash: kinetic, equilibrium, and thermodynamic studies. Ind Eng Chem Res 52(45):15923–15931
47. Mohapatra M, Hariprasad D, Mohapatra L, Anand S, Mishra BK (2012) Mg-doped nano ferrihydrite—A new adsorbent for fluoride removal from aqueous solutions. Appl Surf Sci 258(10):4228–4236
48. Xue F, Xu Y, Lu S, Ju S, Xing W (2016) Adsorption of cefocelis hydrochloride on macroporous resin: kinetics, equilibrium, and thermodynamic studies. J Chem Eng Data 61(6):2179–2185
49. Guerra DJ, Da Silva RA (2014) Kinetic and thermodynamic studies of Brazilian illite–kaolinite in natural and intercalated forms as adsorbents to removal of Zn2+ from aqueous solutions. Journal of the Taiwan Institute of Chemical Engineers 45(1):268–274

Tables

Table 1: Adsorption parameters for Cr^{6+} removal

T (K)	*Langmuir*				
298	$1/q_m$	R^2	K_L (mg L^{-1})	q_m (mg g^{-1})	R_L
	6.481	0.92	0.261	0.154	0.767
Freundlich					
298	1/n	R^2	n	lnK_f	K_f
	0.054	0.11	18.28	0.778	0.459
Temkin					
298	B_T	R^2	lnA_T	A_T	
	24.433	0.99	2.442	0.0869	
Dubinin and Radushkevich (D-R)					
298	q_m (mg g^{-1})	R^2	K (mol^2 J^{-2}) ×10^{-7}	E_m (KJ mol^{-1})	
	4.89	0.34	2.33	1.463	

Table 2: kinetic parameters for Cr (VI) adsorption

Pseudo first order			
60mg/L			
T(K)	k_1	R^2	q_e
298	0.065	0.68	0.98
Pseudo second order			
298	k_2	R^2	q_e
	0.985	0.98	0.139
Intraparticle diffusion			
298	k_i	R^2	X_i
	0.0063	0.79	0.076

Table 3: Various thermodynamic parameters for Cr^{6+} adsorption process

Van't Hoff plot	
ΔG (kJ/mol)	-13.23
ΔH (kJ/mol)	-2.297
ΔS (kJ/mol)	0.045
R^2	0.37

Figures

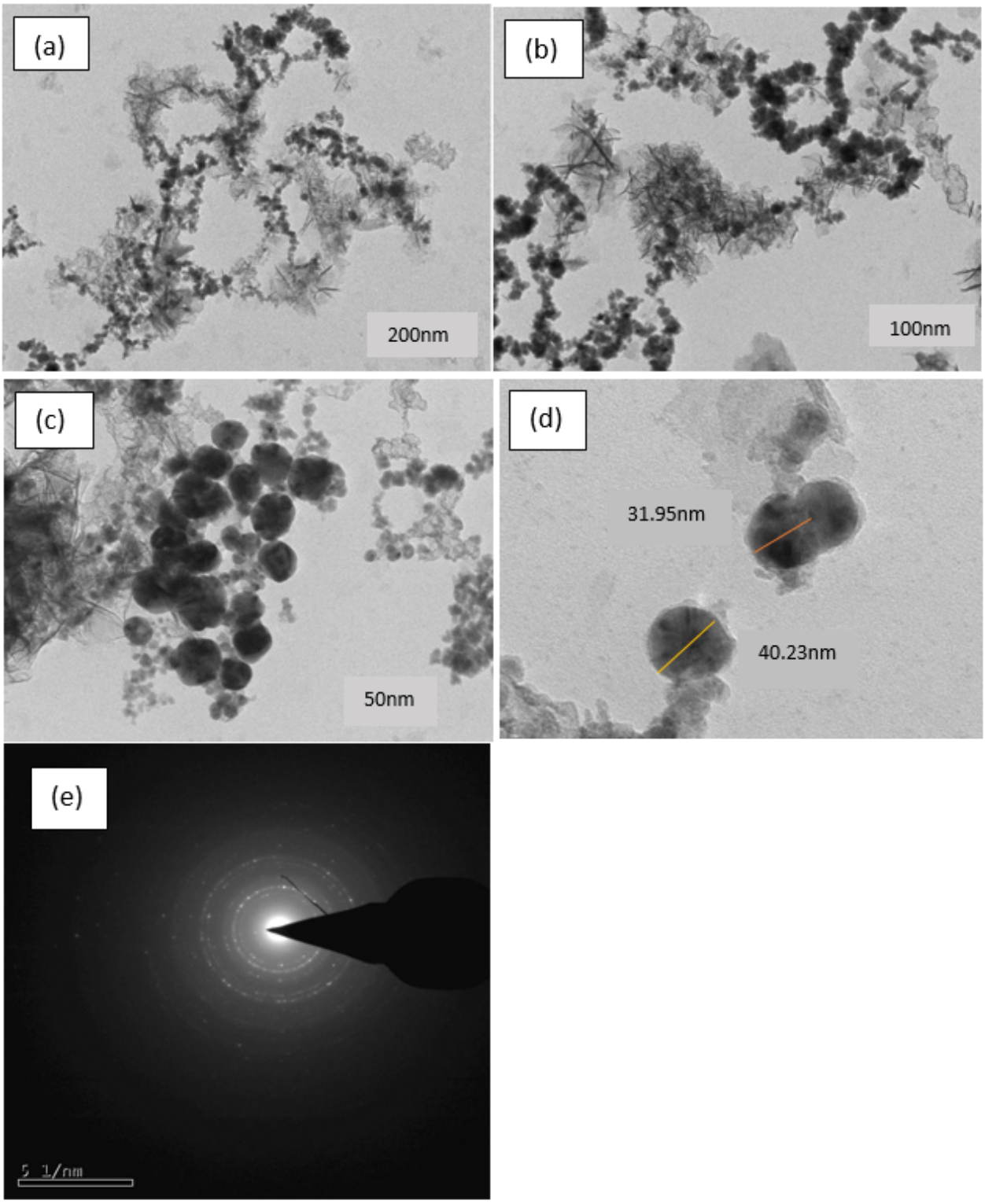

Figure 1

(a-d) TEM images of synthesized Fe_3O_4 nanoparticles (e) SAED pattern of the corresponding nanoparticles.

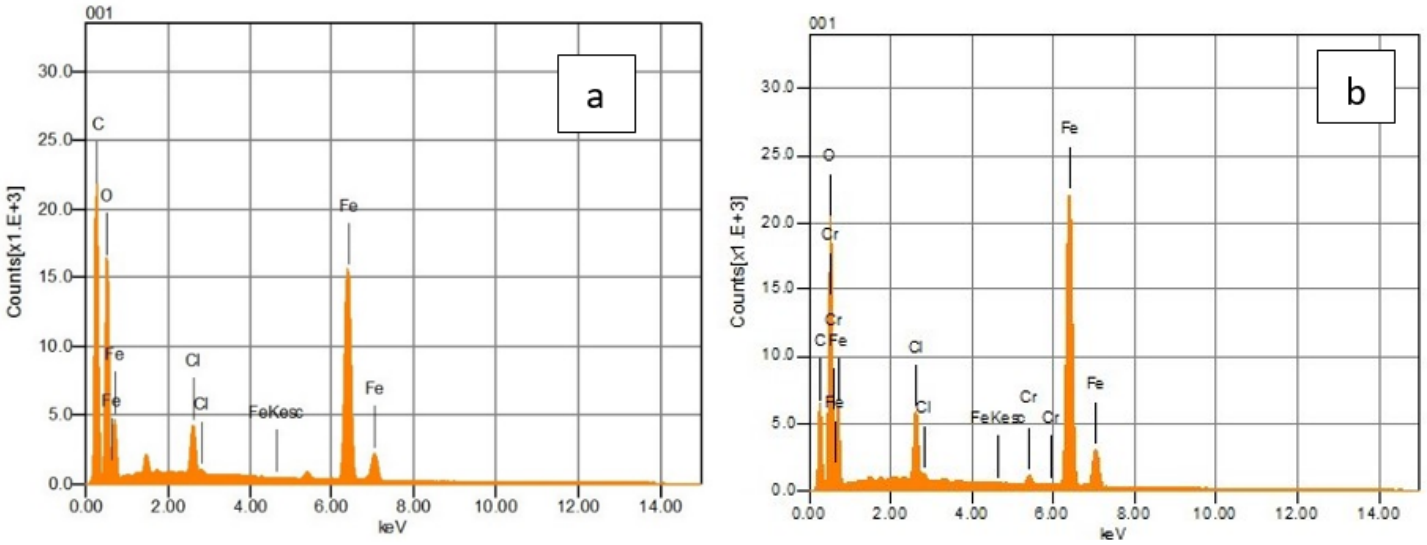

Figure 2

EDX spectra of Fe_3O_4 nanoparticles (a) before and (b) after Cr^{6+} adsorption

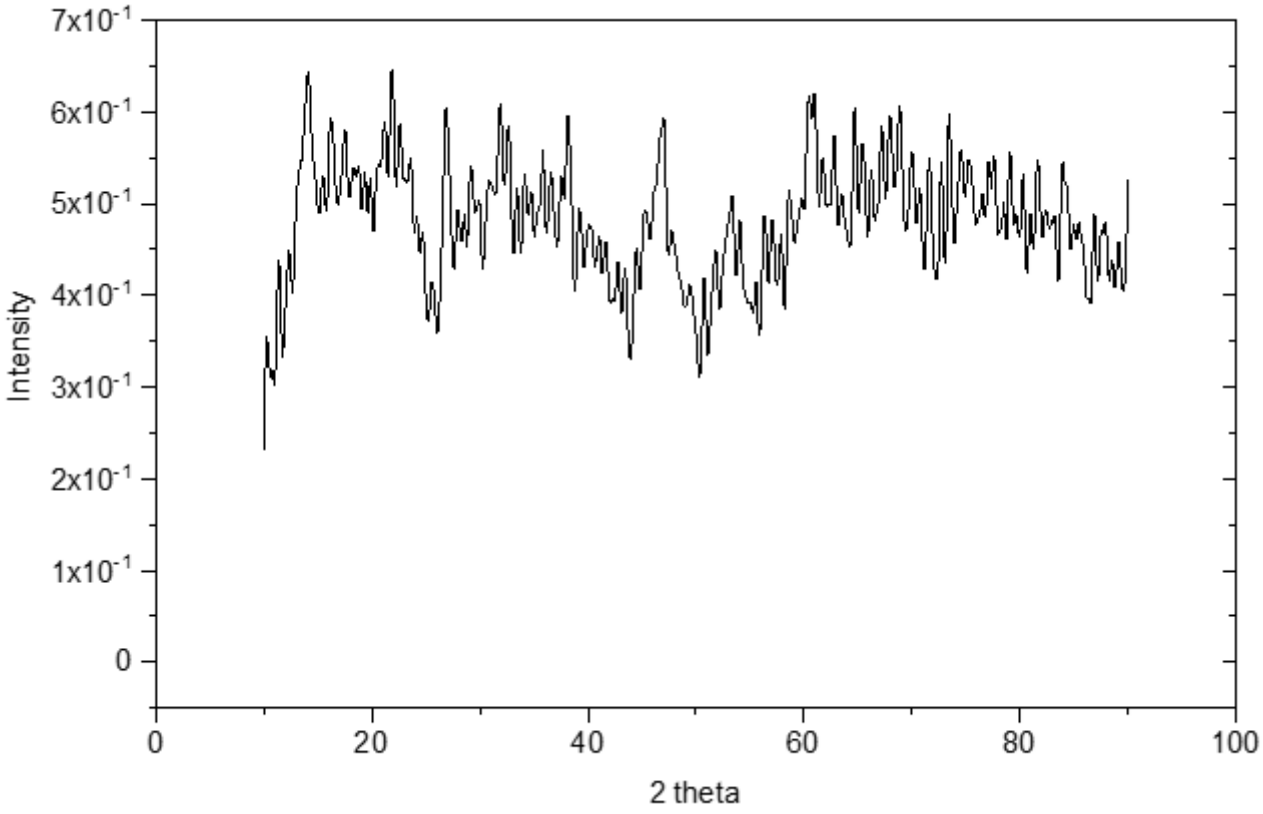

Figure 3

XRD pattern of Fe_3O_4 nanoparticles at different angles i.e. θ=10-90

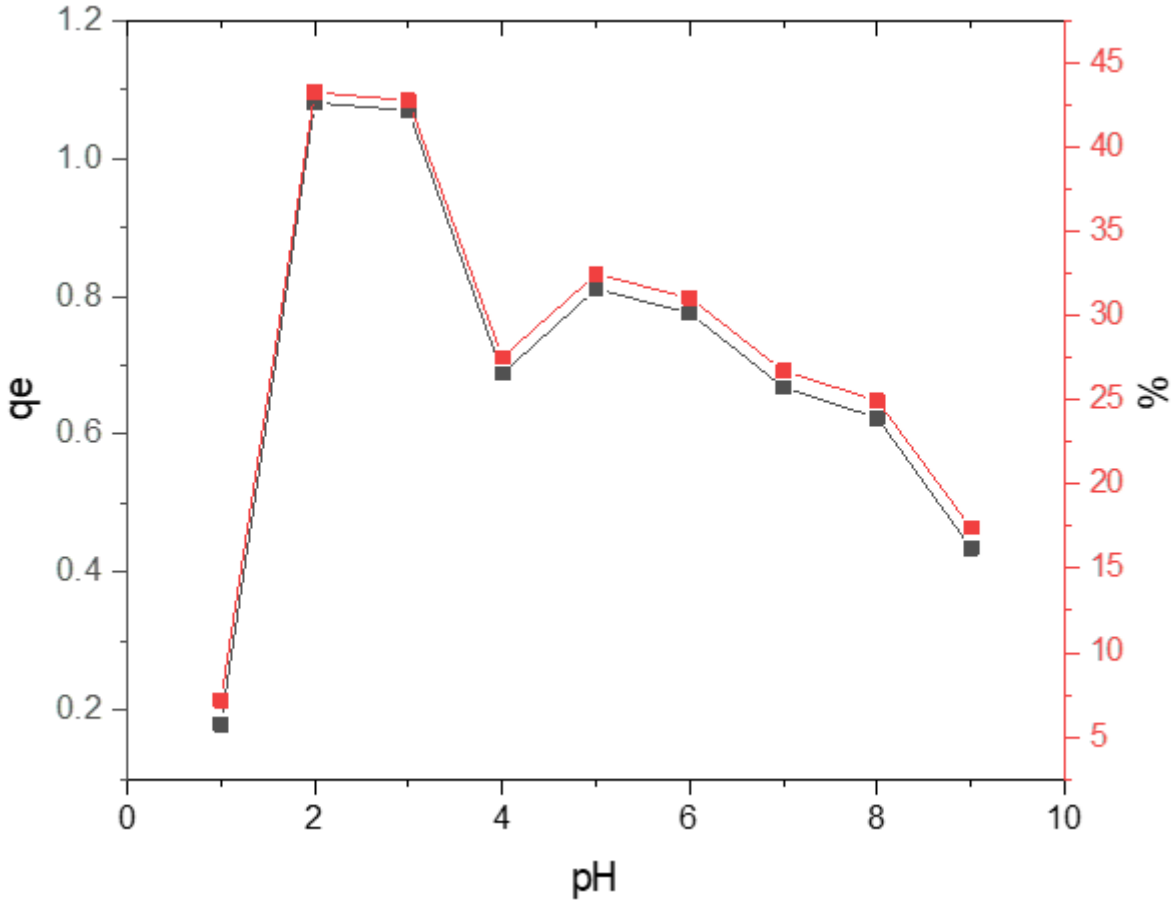

Figure 4

Variation of Cr^{6+} adsorption with pH [adsorbent dose: 20 mg, initial Cr^{6+} concentration: 50 mg L^{-1}, contact time: 30 minutes, temperature: 25˚C]

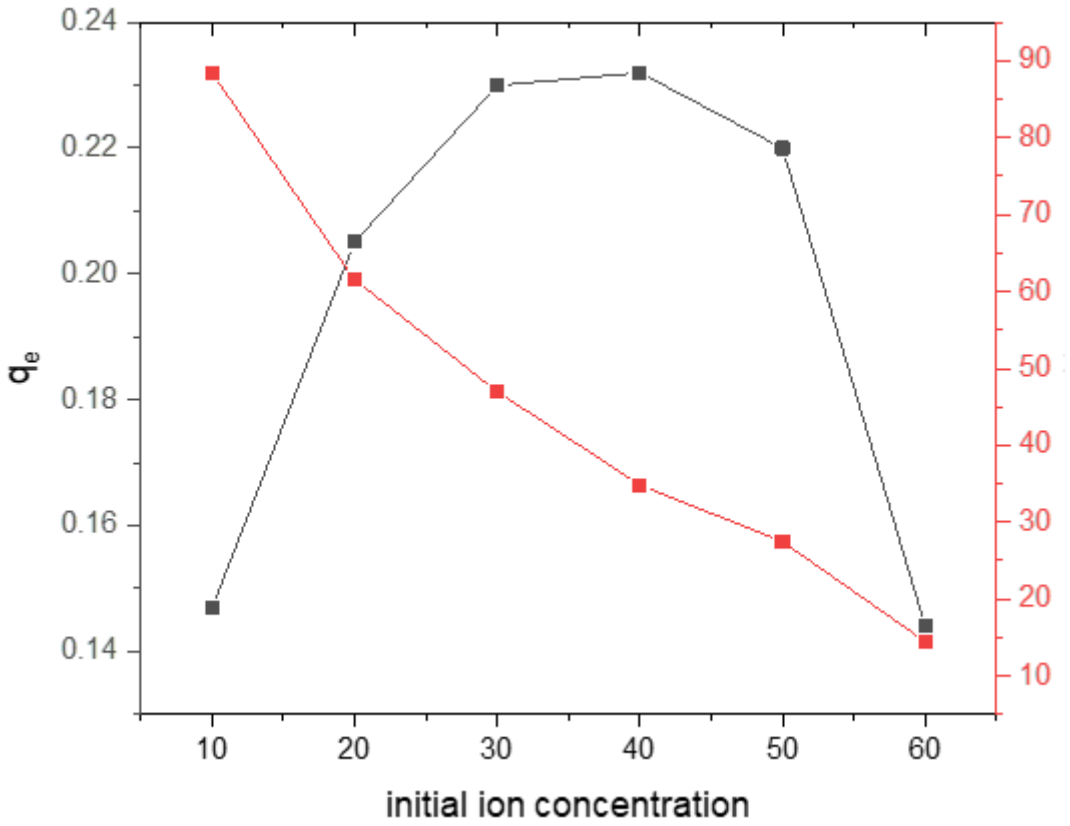

Figure 5

Variation of Cr^{6+} adsorption with initial ion concentration [pH: 2, adsorbent dose: 20 mg, contact time: 30 minutes, temperature: 25˚C]

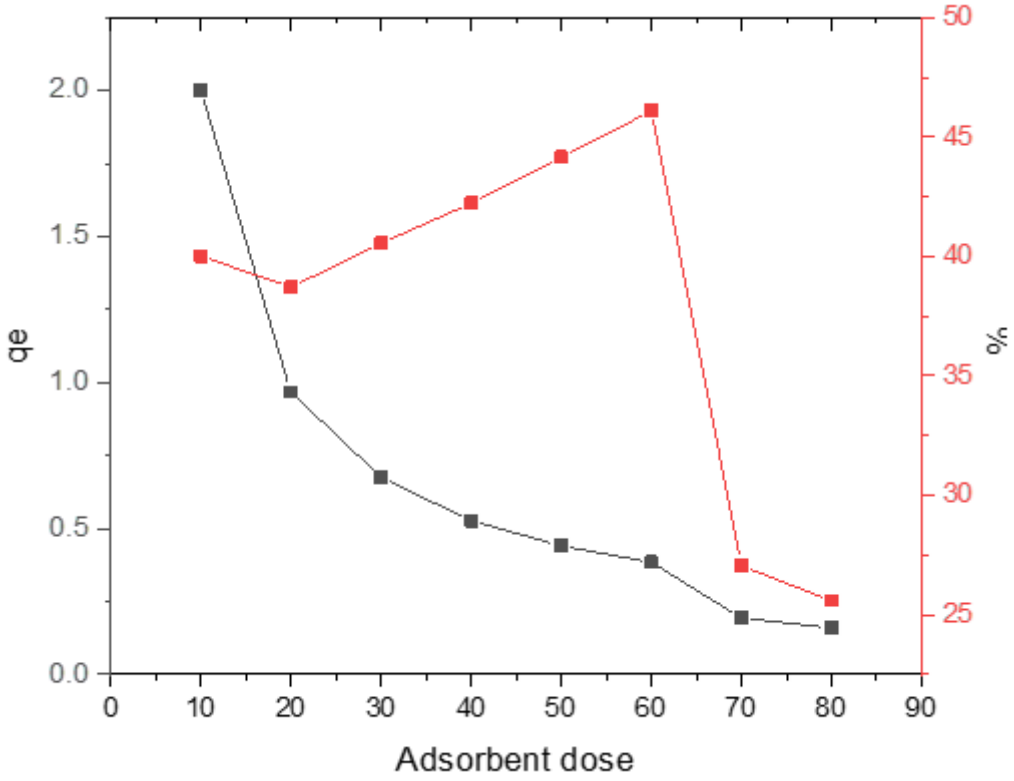

Figure 6

Variation of removal percent with adsorbent dose [pH: 2, initial Cr^{6+} concentration: 10 mg L^{-1}, contact time: 30 minutes, temperature: 25˚C]

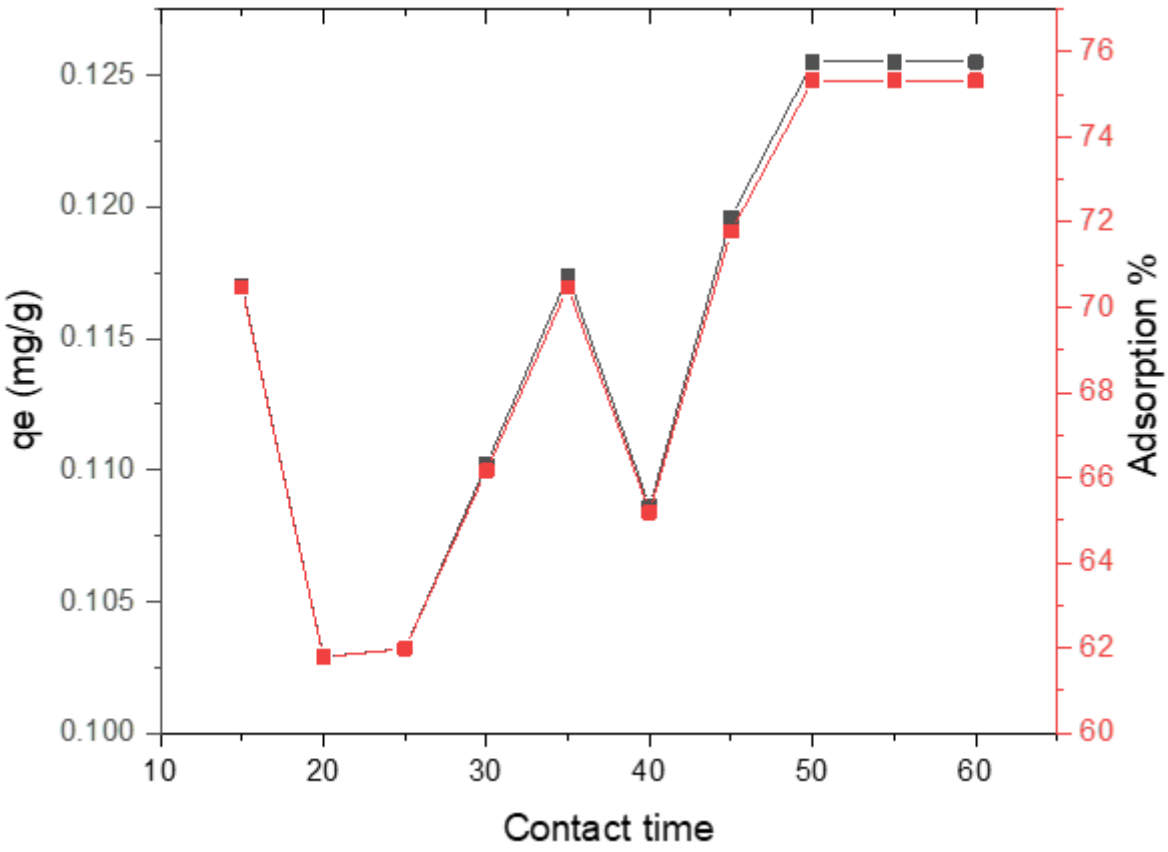

Figure 7

Variation of Cr^{6+} adsorption with contact time [pH: 2, adsorbent dose: 60 mg, initial Cr^{6+} concentration: 10 mg L^{-1}, temperature: 25˚C]

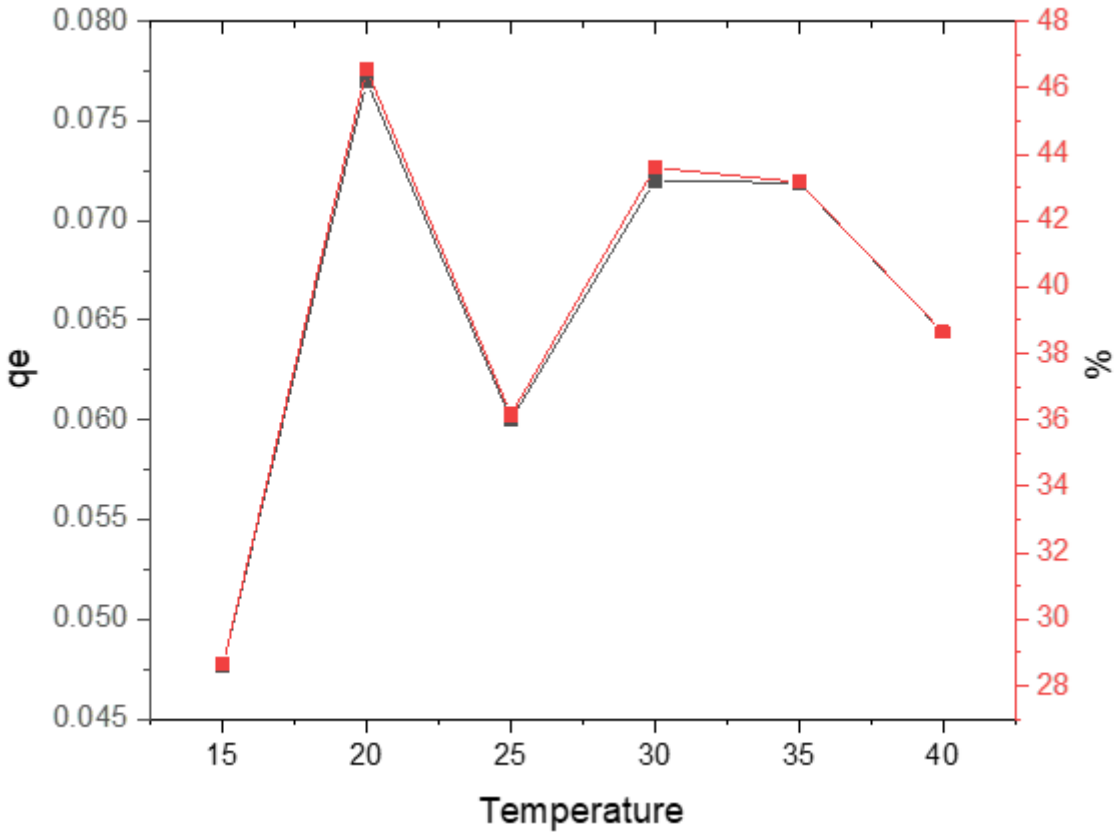

Figure 8

Variation of Cr^{6+} adsorption with temperature [pH: 2, adsorbent dose: 60 mg, initial Cr^{6+} concentration: 10 mg L^{-1}, contact time: 50 minutes]

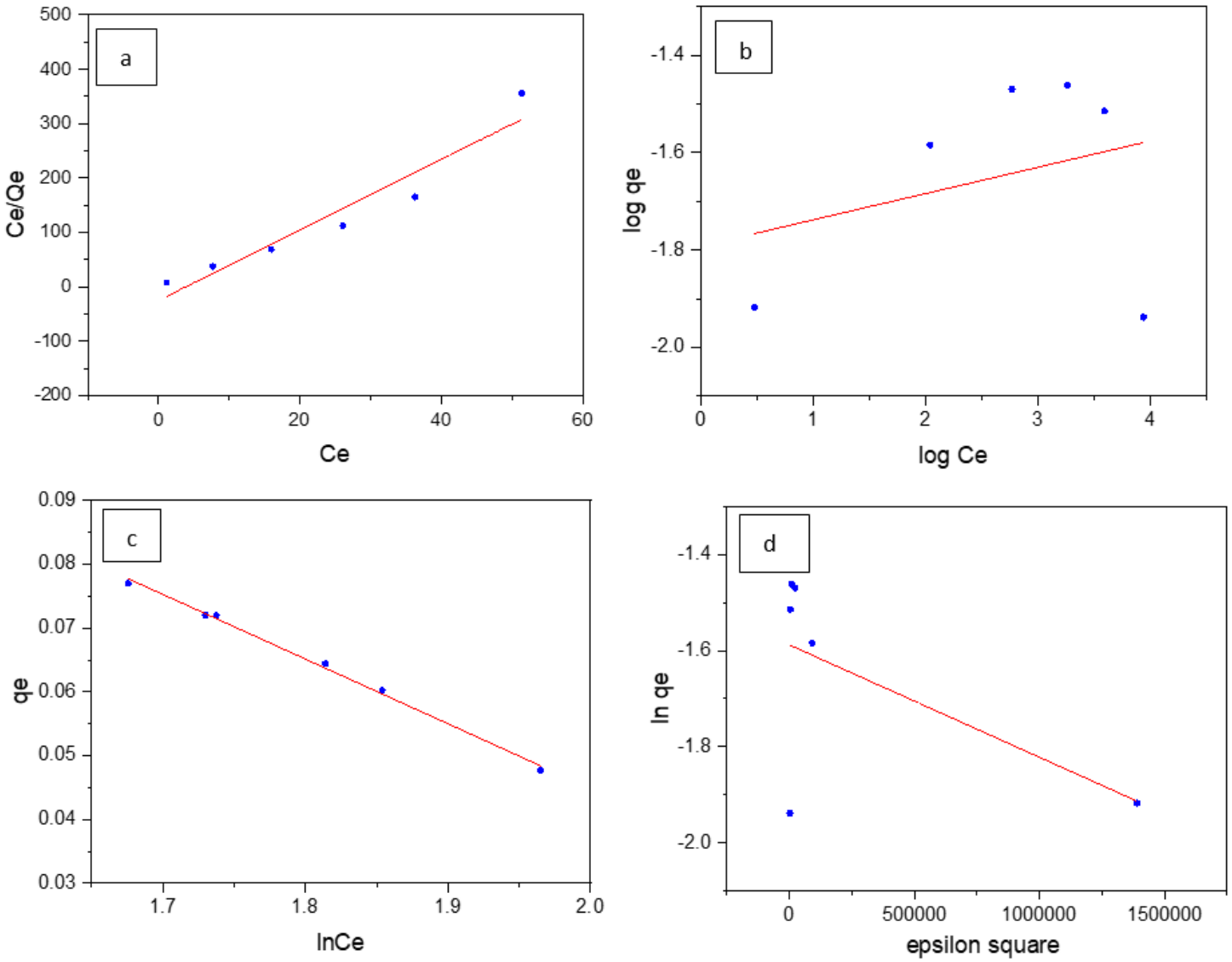

Figure 9

(a) Langmuir isotherm (b) Freundlich isotherm (c) Temkin isotherm

(d) D-R isotherm

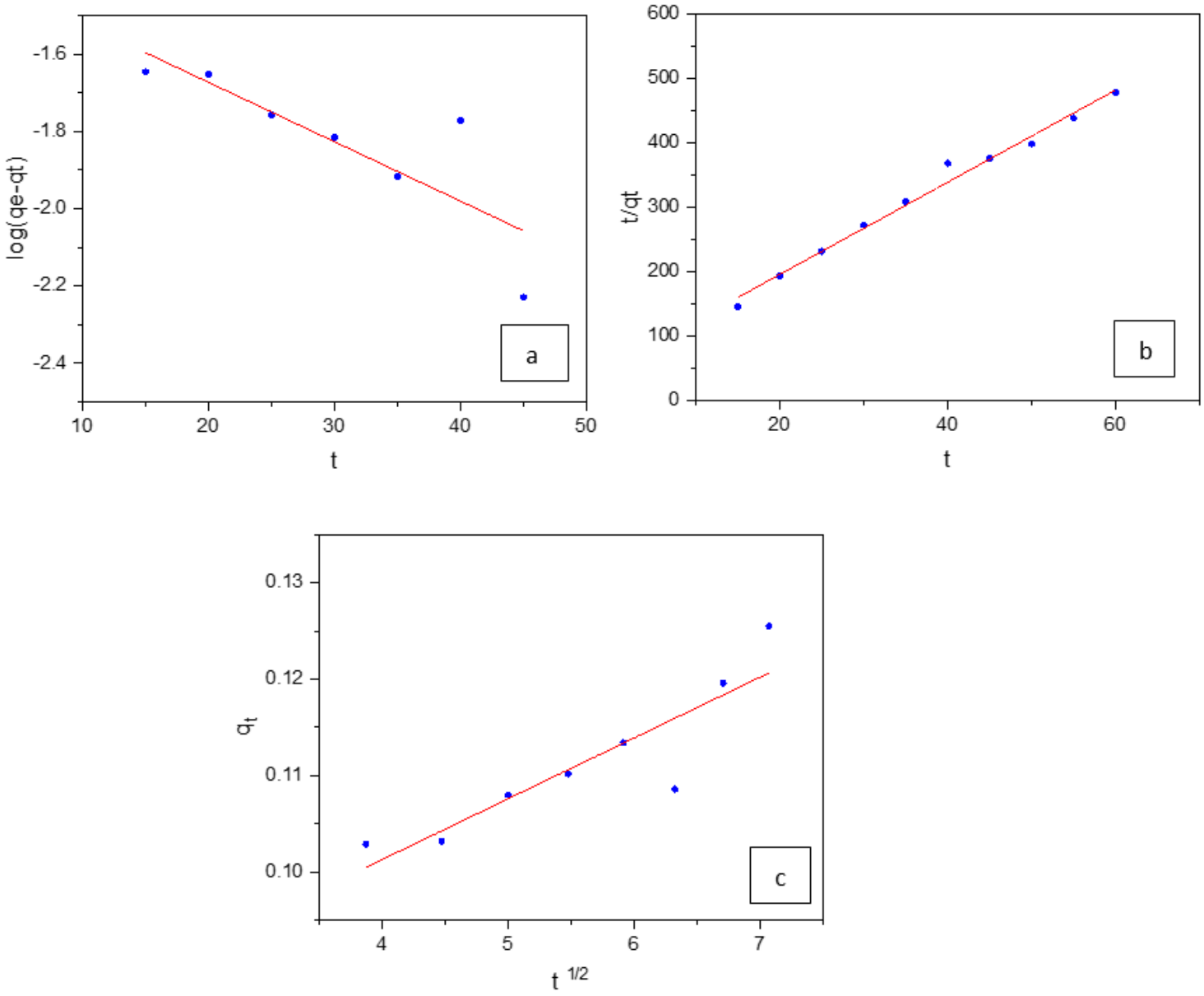

Figure 10

(a) Pseudo first order (b) Pseudo second order (c) Intraparticle diffusion

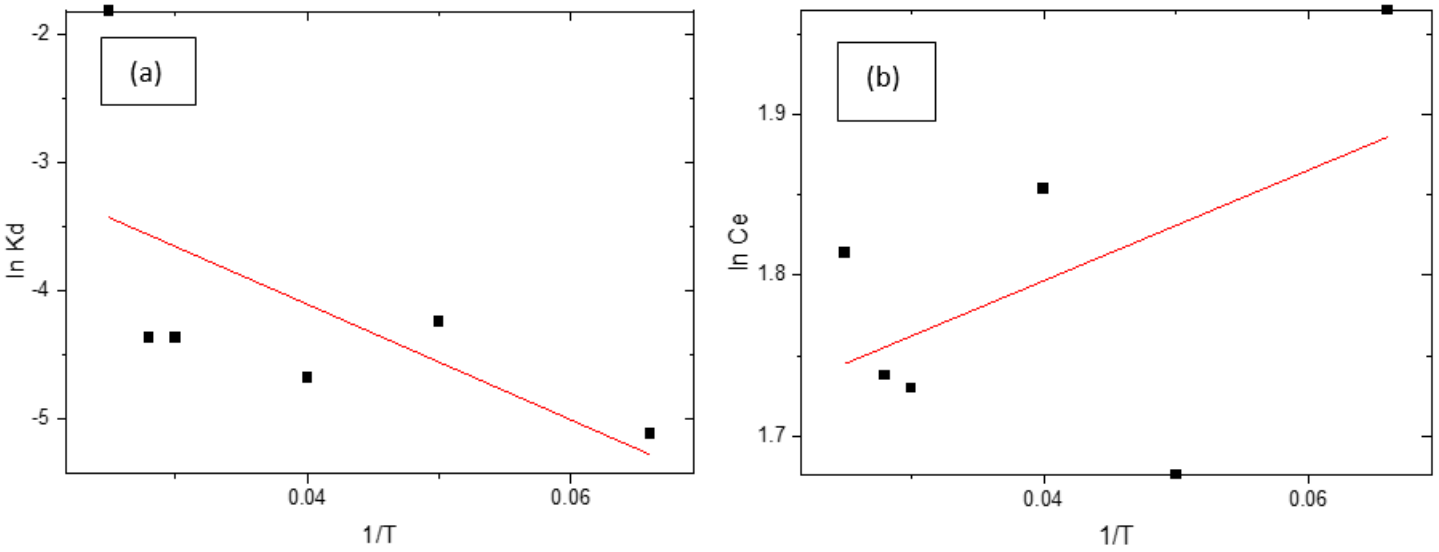

Figure 11

Van't hoff plots for K_d (a) and C_e (b) for Cr^{6+} adsorption

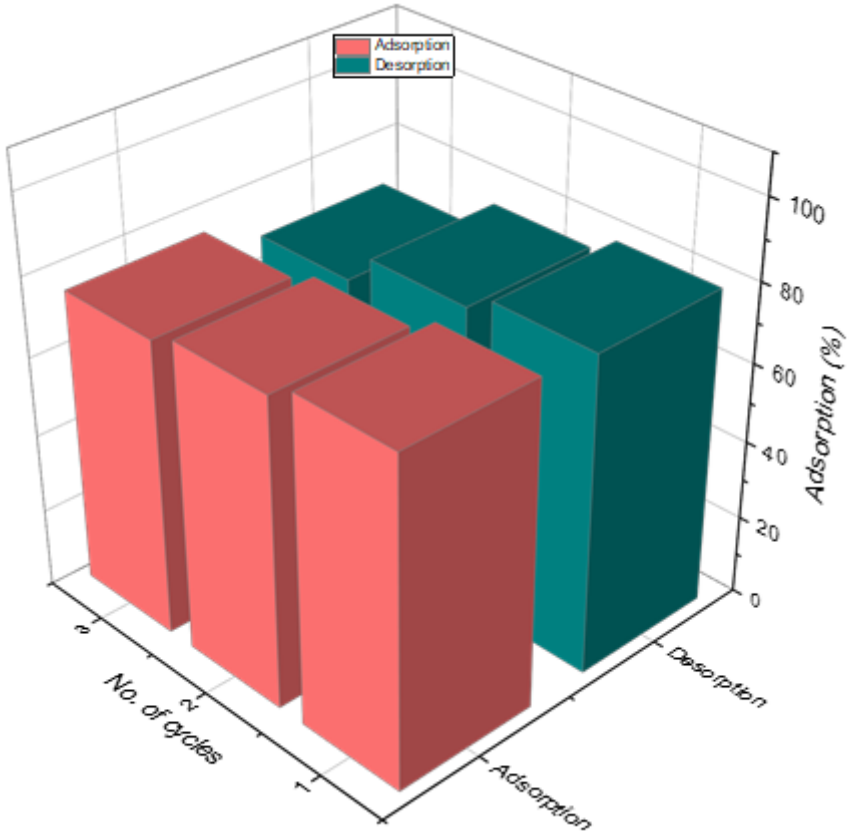

Figure 12

Consecutive adsorption-desorption cycles